UNIVERSITY OF CALIFORNIA SAN DIEGO

A compliant thorax design for robustness and elastic energy exchange in flapping-wing robots

A Thesis submitted in partial satisfaction of the
requirements for the degree
Master of Science

in

Engineering Sciences (Mechanical Engineering)

by

Hang Gao

Committee in charge:

Professor Nick Gravish, Chair
Professor Sonia Martinez
Professor Mike Tolley

2022

The Thesis of Hang Gao is approved, and it is acceptable in quality and form for publication on microfilm and electronically.

University of California San Diego

2022

DEDICATION

To two.

EPIGRAPH

A careful quotation

conveys brilliance.

—Smarty Pants

TABLE OF CONTENTS

LIST OF FIGURES

ACKNOWLEDGEMENTS

First, I would like to express my gratitude to my advisor Prof. Nicholas Gravish for supporting my research so much and giving me the opportunity to work in the lab as a master's student. Every time, when I talked with him in topic meeting and in the lab, I always get something new. His creative and insightful thoughts kept me going. And James Lynch, as my co-author, he gave me a lot of suggestions and research insight. I cannot imagine finishing this project without Nick and James's support. Besides my advisor and James, I would like to thank the rest of my thesis committee members: Prof. Sonia Martinez and Prof. Mike Tolley for attending my defense and for their precious feedback during the course of the project. Other than that, I thank all the members of Gravish Lab for the insightful discussions and for all the fun we had working together in the lab. And I would like to thank my girlfriend for staying with me and giving me moral support. Last but not least, I thank my family for encouraging me throughout this project and supporting my stay at University of California San Diego.

Chapters 1, 2, 3, 4 and 5, in full, are a reprint of the material as it appears in The IEEE Robotics and Automation Letters 2022. Hang Gao; James Lynch; Nick Gravish. The thesis author was the primary investigator and author of this paper.

VITA

2016-2020	Bachelor of Science in Mechanical Engineering , Anhui University of Science and Technology
2020-2022	Master of Science in Engineering Sciences (Mechanical Engineering), University of California San Diego
2022-present	PhD. in Mechanical Engineering, Cornell University

ABSTRACT OF THE THESIS

A compliant thorax design for robustness and elastic energy exchange in flapping-wing robots

by

Hang Gao

Master of Science in Engineering Sciences (Mechanical Engineering)

University of California San Diego, 2022

Professor Nick Gravish, Chair

Flapping wing insects benefit from a compliant thorax that provides elastic energy exchange and resiliency to wing collisions. In this thesis, we present a flapping wing robot that uses an underactuated, compliant, transmission inspired by the insect thorax. We developed a novel fabrication method that combines carbon fiber (CF) laminate and soft robotics fabrication techniques for transmission construction. The transmission design is optimized to achieve desired wingstroke requirements and to allow for independent motion of each wing. We validate these design choices in benchtop tests measuring transmission compliance and kinematics. We integrate the transmission with laminate wings and two types of actuation, demonstrating elastic energy exchange and limited lift-off capabilities Lastly, we tested collision mitigation through flapping wing experiments that obstructed the

motion of a wing. These experiments demonstrate that an underactuated compliant, transmission can provide resilience and robustness to flapping wing robots.

Chapter 1

Introduction and current state of art

1.1 Introduction

In an effort to develop ever smaller high-performance flapping-wing micro-aerial vehicles (FWMAVs), roboticists have looked to flying insects for inspiration [1, 2]. In the last decade, they have achieved major successes including controlled tethered [3,4] and untethered [5–7] flight as well as the integration of sensors [8–10]. However, FWMAVs continue to be relatively delicate, made of lightweight, brittle materials in an effort to maximize strength while minimizing weight. If they are ever to be deployed in the unpredictable environments of the real world, micro flying robots will need to become more robust. As the scale of robots decreases, the space they are working in needs a higher ability to squeeze, stretch and morph

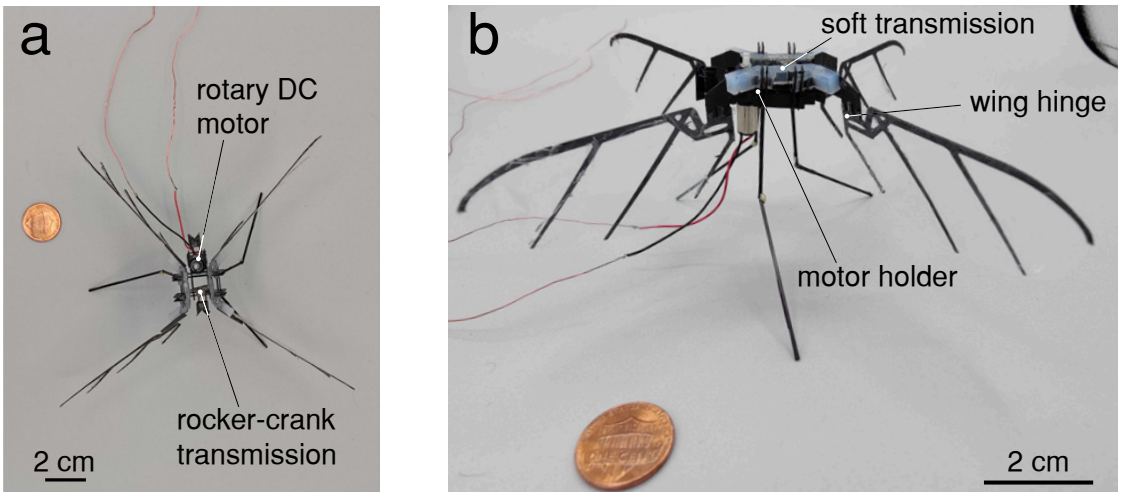

Figure 1.1: A 3.6 gram flapping hummingbird-scale robot with soft transmission. The wing span is 21cm, and the overall dimensions of the robot are 16cm × 16cm when the transmission is in the neutral position.(a) Top view (b) Front view

to adapt to a more complex environment [11].

The compliance of the insect flight anatomy is one factor that helps insects avoid damage that would otherwise cause catastrophic failure. Many insects and other arthropods have highly elastic proteins located in their tendons, wing joints, and in patches of their exoskeleton [12, 13]. Most flying insects flap their wings by transmitting the force of powerful flight muscles through a deformable thorax, which is thought to reduce flight power requirements via the storage and release of elastic energy [14]. The functionality of elastic proteins is not limited to energy storage, however; it also plays a critical role in the flexibility and deformability of the exoskeleton and in the reduction of fatigue and damage in joints, wing veins, and other anatomical elements [13, 15]. Additionally, elastic elements in the thorax are critical for coupling the left-right wing motion in a way that enables wing coordination while also allowing for variation of wingbeat kinematics between

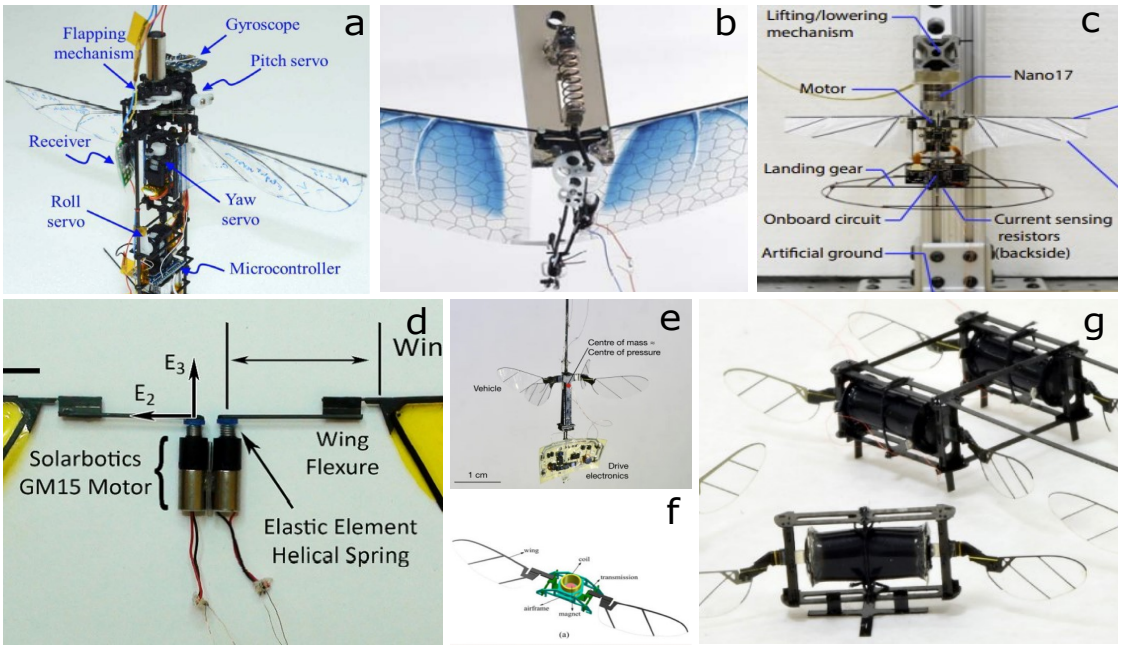

Figure 1.2: Representative FWMAVs. From (a) to (b), traditional slider-crank transmission vehicles: (a)21g insect-like tailless FWMAV [6]. (b)Mass-spring efficient resonant FWMAV [17]. (c) and (d), directly motor-driven FWMAVs:(c)Motor-driven hummingbird robot [4]. (d)CMU FWMAV [18]. From (e) to (g), Four-bar linkage system (with CF laminates) FWMAVs: (e) The RoboBee X-Wing [5]. (f)Electromagnetic FWMAV [19]. (g)Dielectric elastomer actuators (DEAS) -driven FWMAV [20].

left and right wings [16].

Inspired by the elastic elements in insects, and also driven by the engineering promise of resonant efficiency, roboticists have incorporated elastic elements in to FWMAVs [17, 18, 21]. Elastic energy storage and return in the actuation system can improve flapping wing efficiency [22], and the addition of flexible passive wing hinges enables wings to generate lift on both the up- and down-strokes without requiring direct control of the wing pitch [20]. However, most attempts at incorporating elastic elements have maintained rigid linkages between wing and actuator, with a spring in parallel [23]. Thus, the kinematics of the wings are directly cou-

pled to the kinematics of the actuator(s). This tends to simplify control, but it also means that any collisions are transmitted directly back to the actuator. We believe that incorporating further compliance in the transmission of a FWMAV may lead to improved resilience and flight performance.

In the following work, we develop a compliant, underactuated, transmission for flapping wing robots. The goal of this transmission is to provide elastic energy exchange and robustness to collisions for a robot. We first present a new fabrication method for this transmission and the full four-winged robot (Fig. 1). Next we perform benchtop characterization experiments of the components as well as lift-off and performance measurements of the robot. Lastly, we discuss the implications of this work and limitations still to overcome.

Chapter 1, in full, is a reprint of the material as it appears in The IEEE Robotics and Automation Letters 2022. Hang Gao; James Lynch; Nick Gravish. The thesis author was the primary investigator and author of this paper.

Chapter 2

Design

2.1 Robot Design

Our robot is comprised of four main elements: 1) a compliant thorax, 2) a set of four wings, 3) an actuator; either linear voice coil or rotary DC micro DC motor, and 4) a chassis and legs. An overview of these components and the fabrication methods employed can be seen in Figure 2.1. In the following section we describe the design and fabrication of these components.

2.1.1 Transmission

Kinematic design

To enable wing robustness and mitigate the effects of wing-structure collisions, we selected an underactuated transmission design that maps the single linear actu-

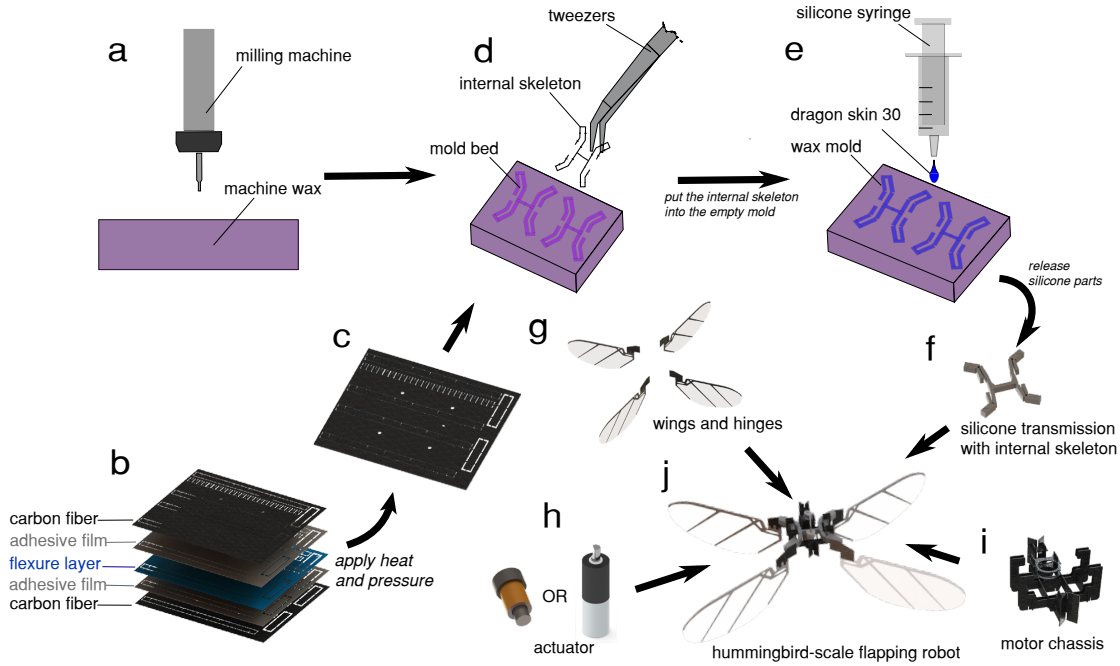

Figure 2.1: Overview of the manufacturing process. (a) The wax mold for the compliant transmission was machined using a 1/32" flat end mill in an Othermill micro-milling machine. (b) The skeleton of the transmission is a laminate constructed from a 5-layer stack of CF, adhesive, and thin, flexible polymer (c) We apply heat and pressure to fuse the laminate, pop out the skeleton, and fold it into the proper shape. (d) The CF internal skeleton was placed into the mold bed, held in place by small horizontal tabs to prevent misalignment. (e) Mold was filled with silicone (Dragon Skin 30, Smooth-On) using a syringe to ensure an even fill. After setting completely, the compliant transmission (f) was assembled with the wings (g), actuator (h), and motor chassis (i) into the completed FWMAV (j).

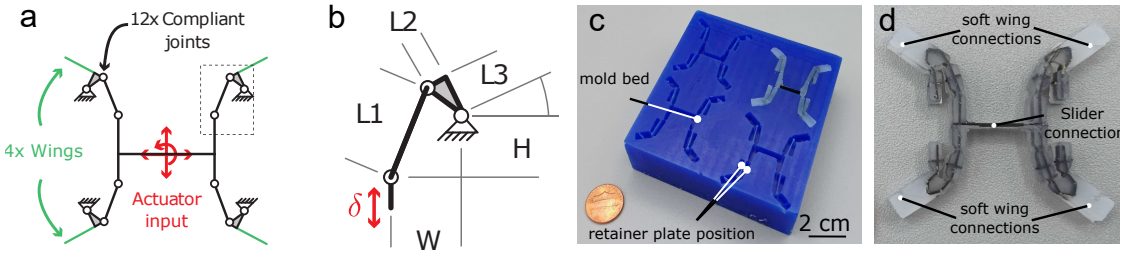

Figure 2.2: Kinematics and assembly of a compliant "thorax." (a) Quad-four-bar linkage system that transmits linear actuation to rotational wing motion. White circles indicate flexure joints, green lines indicate wing locations, and the linkage is fixed to the chassis on the sides. (b) Details of the linkage, $L_1 = 4.2$ mm, $L_2 = 2.0$ mm, $L_3 = 0.8$ mm, $W = 3.0$ mm, $H = 3.13$ mm. (c) Photo of the machined wax mold. (d) Completed transmission with carbon fiber skeleton and Silicone mold.

ator across a parallel linkage to multiple wings. To further illustrate the potential of such an underactuate structure, we chose a four-wing configuration (Fig. 2.2). The transmission kinematic design is inspired by the single-actuator Harvard microrobotic flying insect [24] which uses a symmetric dual-four-bar linkage system to generate wing motion. The actuator is attached to the central link of the transmission and drives the four linkages with a periodic force signal. The linkage lengths, L_1, L_2, and L_3 were optimized numerically to maximize wing sweep angle for the specified actuator stroke (Fig. 2.2a), and the transmission was designed to be supported by a CF chassis (see *Chassis and structure* section below).

To determine the link lengths for our transmission we used numerical optimization to optimize for symmetric wing motion with maximum desired amplitude under the input actuation constraints. We use $fmincon()$ in MATLAB with optimized parameters as $3 < L_1 < 4.2$, $2 < L_2 < 5$, $0 < L_3 < 5$, and initial

conditions set as [5, 8, 3] for L_1, L_2 and L_3. By optimizing, we derived the length as [4.2,2.0,0.88], inspection with small difference, we use $L_{1,2,3} = [4.2, 2.0, 0.8]$ as the transmission kinematics coefficients.

Initially, we designed the transmission out of silicone alone, but we found that the lack of rigid structure made driving the system challenging. The actuator tended to deflect the silicone locally, resulting in poor force transmission. The solution was to embed a carbon fiber laminate skeleton into the molded silicone (Fig. 2.2c). To maintain the compliance we sought from the silicone, the connection points for the wings remained 100% silicone, while the motor connection was 100% CF, leading to some series-elasticity between actuator and wings. The resulting kinematics are shown in the *Results* section below (Fig 2.3 b). In fact, we note that adding Silicone to CF+Kapton components has been done before (Rosen et. al. [25]), however in that previous work it was a very light coating, not a mold as we present here.

Fabrication

The fabrication of our compliant thorax required the combination of two different fabrication methods: small-scale, high-precision silicone molding for the elastic components and smart composite manufacturing (SCM) methods [26] for the creation of the rigid internal skeleton. We developed a hybrid fabrication process inspired by shape deposition manufacturing [27] that supports flexibility at wing joints and structural rigidity in the body elements.

The fabrication of our transmission includes two steps: 1) we use the SCM method to form the "skeleton" of our transmission, and 2) we mold a protective silicone layer over the transmission (Fig. 2.1a-f). The internal skeleton thus defines the approximate "rigid" kinematics of the transmission, while the protective silicone layer dictates the elasticity of the structure and provides a resilient, protective layer. In previous work, Zhou & Gravish [28] developed a process for centimeter-scale silicone structures that used milled machine wax templates for casting. In the work we extended this process to incorporate the internal skeleton.

The skeleton was fabricated via a typical SCM process (Fig. 2.1b-c) wherein 3D models of the laminated transmission were split into CF (0.2mm thickness), heat-sensitive adhesive (Pyralux 1500), and kapton (25.4micron, 100HN) flexure layers and cut using a DPSS laser (DCH Laser, Photonics Industries). The layers were then aligned and heat pressed (50 psi, 350^{o}F, 30 minute ramp up and down, 2 hour hold) before a release cut freed the components of the skeleton. The components were then assembled into the final structure by hand and prepared to insert into the mold.

Silicone casting molds (Fig. 2.2d) were fabricated out of machine wax (High-Speed Machining Wax, Bantam Tools) using a Micro Mill (Othermill, Bantam Tools Desktop PCB Milling Machine). The wall thickness of the silicone was set to 3.5cm, which was determined via elasticity and blocked force requirements of the transmission discussed later in Fig. 2.5. To determine the mold geometry we computed the geometric "footprint" of the silicone transmission in Solidworks and

then converted to G-code. The machining was performed with a 1/32" diameter flat end mill. The machining depth was constant and held at 3.5cm which provided a flat planar surface for the top and bottom of the transmission. To center the skeleton within the silicone mold, we added four carbon fiber tabs on each side as retainer plates on the wall of the mold to constrain the skeleton along the center line of the transmission. This ensures that the kapton joints of the internal skeleton align perfectly with the silicone compliant joints (Fig. 2.2c,d).

We tested a range of silicone materials (Dragon Skin 10-60, Smooth-On). After a series of tests (See Results and Fig. 2.5a) we ultimately found that Dragonskin 30 performed best for our purposes. We injected the silicone liquid into the mold using a syringe with a 0.8cm diameter nozzle to fill the space between the CF skeleton and the mold, then degassed the silicone in a vacuum chamber with -0.07 atmospheric pressure lasting for 20 minutes to remove air bubbles. We then allowed the silicone to cure for 16 hours before removing and testing. The completed transmission was released from the mold using tweezers, taking care not to damage the silicone (Fig. 2.1e-f).

2.1.2 Wings

Wing Geometry

Insect wing shape, size, and structure vary widely [29]. We chose not to directly mimic any specific insect wing, and instead follow the wing shape of previously

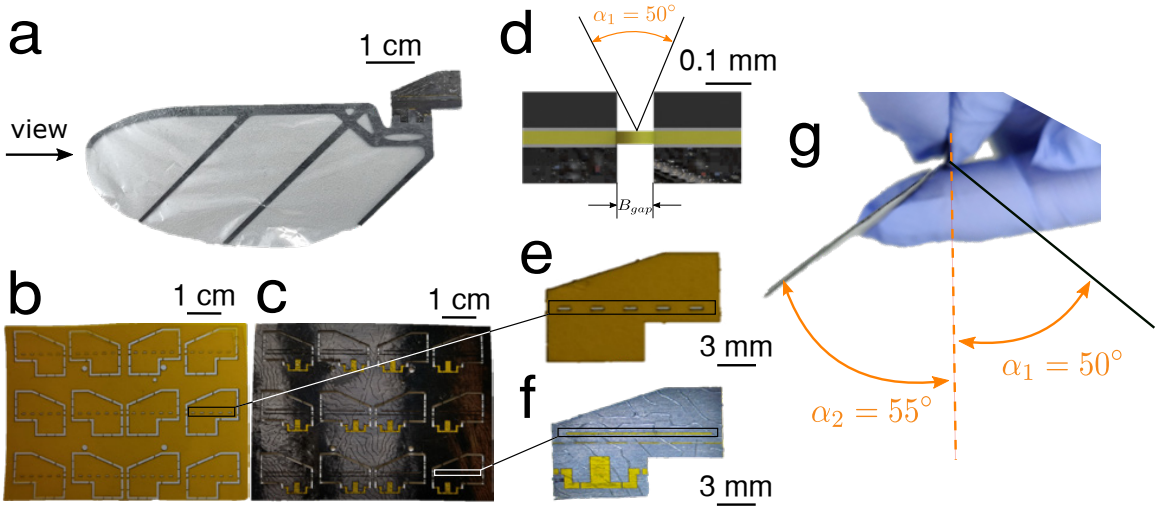

Figure 2.3: Robot wing and hinge design. (a) Side view of wing structure with wing frame and passive hinge. The hinge is constructed as a laminate with flexure (b) and CF layers (c) laminated with adhesive layers (Pyralux 1500) (d) Cross-sectional view of wing hinge indicating mechanical stop angle (e) New Kapton membrane was cut off raster-like space to decrease the stiffness of hinge structure to increase the acceleration of angle-of-attack when flapping. (f) We added a groove to the wing to wick any glue spillage to protect the wing hinge gap from interference from glue. (g) The mechanical stop ensures that angle-of-attack at two mid-stroke is near 50° in both directions

developed MAVs including the Harvard RoboBee [3] and the UW Robofly [30]. The wing structure is composed of transparent thin polymer (5μm thickness) supported by a CF frame with a thick leading edge and spars to support the trailing edge (Fig. 2.3a), and it was fabricated using SCM lamination methods.

Wing Hinge

Insects and hummingbirds pitch their wings so that they can produce lift on both upstroke and downstroke [31]. We implemented passive CF laminate wing hinges to achieve this effect without requiring direct control of the wing pitch (Fig. 2.3b-f. To generate higher lift, we designed the wing hinge with a mechanical stop as a pitch angle constraint. As shown in Fig. 2.3d, we designed the gap of the hinge $B_{gap} = 0.08$mm based on the thickness of the carbon fiber sheet to make two sides of the carbon fiber part collide when the wing pitch reaches $\approx 50°$. In practice, the wing tends to hit the mechanical stop at 50° in one direction and 55° in the other (Fig. 2.3g. The simulation work from Whitney & Wood [2] shows the $45° \rightarrow 65°$ range angle-of-attack at mid-stroke will result in lower aerodynamic damping and better efficiency, assuming sinusoidal flapping and symmetric sinusoidal wing pitching).

2.1.3 Actuation

An important step for achieving flapping wing flight is the selection of an actuator. A variety of actuation schemes including piezoelectric (PZT) bending

actuators [3, 5], soft DEA actuators [20], small DC Motors [17, 18], and electromagnetic coil actuators [32] have been used for small-scale flapping flight. PZT actuators and DEAs have relatively high power density (DEA has 300W/kg and a lifetime of over 600,000 cycles [20]). However, PZT is fragile and DEA is hard to fabricate, and both require extremely high actuation voltages. A voice coil motor as an oscillating electromagnetic actuator can generate a linear motion with a relatively higher power density (15kw/kg) [19], so we chose. DC motors are cheap, well developed, and have a linear relationship between current and force with fixed voltage. To focus on a design that incorporates a voice coil as our primary linear actuator. And then, aiming at lift force and universality, we tried to focus on rotary motor. Thus, We tried two different actuators: a linear voice coil actuator and a micro rotary DC motor.

There were two additional important reasons for selecting a rotary actuator. The first, although linear motions controlled via a DC motor and slider-crank assembly have a fixed amplitude, however, our silicone transmission can still amplify the amplitude of wing flapping angle at resonance by soft silicone transmission joints even with fixed input slider stroke. Second, even though the slider-crank excess longitudinal component force on slider when we apply the slider on horizontal motion. But we can also solve the longitudinal component force by set an offset position for the slider, and the silicone transmission itself can also tolerance some of the longitudinal component force.

We used a small voice coil motor, (LVCM-010-013-01, Moticont). The weight

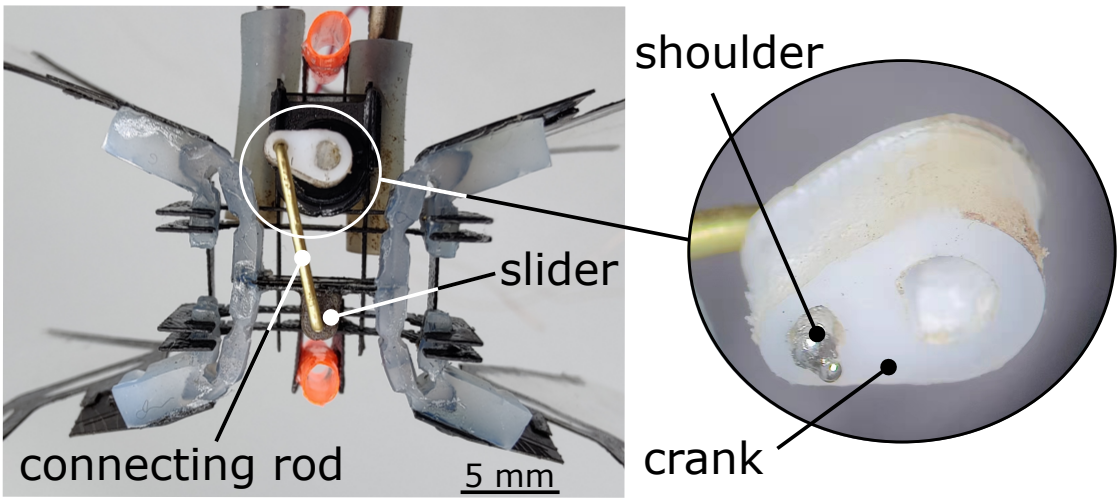

Figure 2.4: Close-up view of the slider crank

and the scale of the motor is relatively low, which is critical as it makes up the bulk of the overall mass of the robot (63.3 %). The magnetic core is the only moving part of the linear actuator, and it is fixed to the carbon fiber cross-bar on the transmission. The core has a lower mass than the wire coil assembly, so it generates relatively lower inertial effects as it moves back and forth. The rated stroke of the motor is 6.4mm, although in practice the stroke is closer to 3.3mm after incorporating it with the transmission and chassis using high temperature tolerance paste(J-B Weld 37901).

For DC motor case, we utilized a micro DC motor, (136:1 Sub-Micro Plastic Planetary Gearmotor). And the stall torque is 550 grams/cm at 6V. The weight makes up the bulk of the overall mass of the robot (41.67 %). As shown in the Fig. 2.4, to decrease the friction on the slider-crank, the rotary motor transfer the

torque to a Slippery PTFE crank (9266K83, McMASTER-CARR) of the slider crank, and we choose a formable brass rod (8859K481, McMASTER-CARR) as connecting rod, and set the revolute joint (Slippery Delrin material, 8578K411, McMASTER-CARR) onto the carbon fiber cross-bar on the transmission as slider, to make the input motion moves back and forth. In practice, the stroke is 5.2mm totally. Other than that, to maintain the brass rod connected with the crank in-plane, we use soldering on the tip of the rod as a shoulder of the rod. As shown in the Fig. 2.4 zoom-in, which is the bottom view of the robot prototype.

2.1.4 Chassis and structure

The chassis forms the primary structure of the robot. It has two purposes: 1) Support the actuator and transmission and 2) provide attachment points for legs and guide rail support structures during vertical lift experiments.

Initially, we used a 3D printer to create the motor chassis. However, that version had two disadvantages: thermal tolerance and mass density. The heat (over 150°C after running the voice coil for 10 seconds with $3A$ current) produced by the voice coil motor can quickly melt the PLA material structure. Therefore, we designed the motor chassis out of carbon fiber, like the transmission's internal skeleton. The motor chassis is composed of carbon fiber sheet (0.25mm thickness) assembled via slot joints and fixed using cyanoacrylate glue (Loctite 495) to create a rigid structure(Fig. 2.1 i).

2.1.5 Assembly

Once all individual components were fabricated we assembled the robot manually. We first attached the transmission to the chassis (Fig. 2.1f,i) using alignment tabs and securing with cyanoacrylate (CA) glue. Once the transmission was secured, we inserted the actuator. Then for voice coil motor case, we glued the magnetic core to the transmission using CA glue and is held within the chassis by a press fit design. For rotary motor case, we glued the revolute joint (Slippery Delrin material, 8578K411, McMASTER-CARR) part onto the carbon fiber cross-bar on the transmission. Furthermore, we plug brass rod as slider-crank connecting rod to the Delrin revolute joint part and the PTEE crank. As shown in Fig. 2.2d, in the cross-bar of the silicone transmission, there is a carbon fiber circle holder for the magnet core. This circle has the same diameter as the magnet core, and we use the high heat tolerance paste (J-B Weld 37901) to align the core and transmission together as concentric circles. Then, we clamped the the motor coil to the motor holder circle of the motor chassis with the first motor holder circle along with the motor edge, to make sure that we can set the magnet core in the neutral position (Fig. 2.1h, i). And for rotary motor case, we computed the length of the brass connecting rod by setting the silicone transmission in the neutral position in SOLIDWORKS, to make sure the slider-crank moves the same distance for back and forth motion. And we adjusted the small offset distance of the slider by excited the silicone transmission motion with power supply, until the four wings flap with

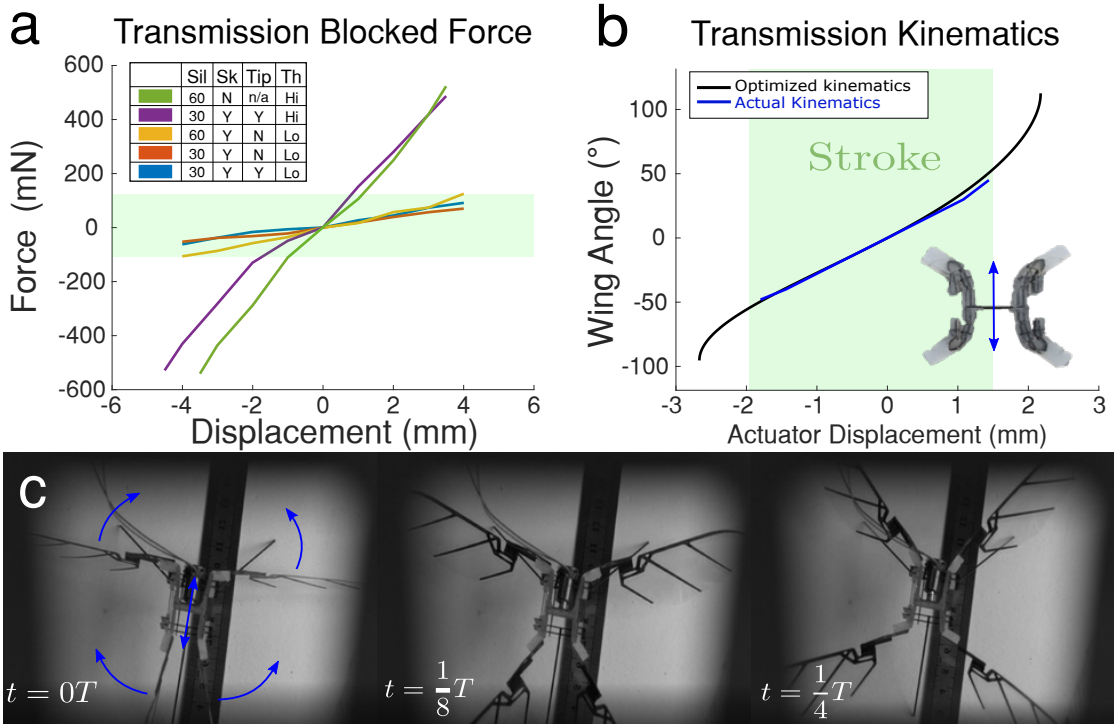

Figure 2.5: Dynamics and Kinematics of the Silicone Transmission. (a) Blocked force necessary to induce displacements for different designs of the transmission (see text) (b) Transmission kinematics, with linear relationship between actuator displacement and flapping magnitude (blue) and optimized curve (black). (c) Video stills show wing motion over 1/4 of a period, T using the linear voice coil actuator

the same angle. At last, we use soldering to add an shaft shoulder on the tip of the connecting rod to limit the motion between connecting rod and crank.

The wings were then attached to the wing hinge along the yellow region on Fig. 2.3f by CA glue, and the wing hinge was glued onto the transmission at the locations indicated in Fig. 2.2a. Lastly, carbon fiber legs were glued to the chassis.

Chapter 2, in full, is a reprint of the material as it appears in The IEEE Robotics and Automation Letters 2022. Hang Gao; James Lynch; Nick Gravish. The thesis author was the primary investigator and author of this paper.

Chapter 3

Results

3.1 Experiment Results

3.1.1 Transmission kinematic and dynamic characterization

In our first experiments, we sought to characterize the force and kinematic behavior of our transmission. We constructed transmissions using silicone of different stiffnesses (Dragon Skin 30 and 60, Smooth-On) and measured the force it takes to deflect the transmission under compression and extension. We also measured the kinematic relationship between input displacement and output wing motion.

We mounted the transmission into the motor chassis and fixed it to a linear XYZ stage (Thorlabs, M-DS40). We mounted a strain gauge (Eujgoov, 0-100g, 0.010%-0.020% accuracy) to a motorized translation stage (Thorlabs, MTS50-ZB) with

3D printed gripper and attached the other end to the cross bar motor connection of the transmission. Starting in the neutral position, we moved the motorized stage, measuring displacement and force from the strain gauge (NI USB-6003, 1 kHz sample rate).

Fig. 2.5a shows the results of the experiment using different versions of the transmission. Ideally, we want to transmit 100% of the motor force to the wings, so we want to minimize the force it takes induce a certain displacement. The green region in the figure indicates the case where it takes less than 200 mN to deflect the cross bar.

We tested 5 different transmission designs using one of two types of silicone, Dragon Skin 30 or 60 ("Sil"). One design was 100% silicone (no skeleton), and the rest had some kind of CF skeleton ("Sk"). For the designs that had a skeleton, some had skeleton going out to the wing connections (Tip = Y) and some had skeleton only at the cross bar motor connection (Tip = N). Finally, we had two thicknesses for the compliant silicone joints; "Hi" indicates a thick joint ($>$ 1mm) and "Lo" indicates a thinner joint ($<$ 0.9mm) (see Fig. 2.2b and d).

We found that lowering silicone joint stiffness improves the performance of the transmission, as does incorporating a rigid skeleton. We also found out that while Dragon Skin 60 compressed very easily, it was more viscous than Dragon Skin 30, which could hinder elastic energy exchange. Moreover, in the rest of the experiments, we concluded that including only a rigid cross bar (Tip =N) leads the silicone transmission to be deeply stretched when driving at high frequencies, which

further decrease the magnitude of flapping. The final configuration is therefore constructed with Dragon Skin 30, a full skeleton, and thin silicone joints.

We optimized the kinematics of silicone body length with L_1, L_2, L_3 as [4.2,2.0,0.8] mm and then derive the linear relationship in full stroke between actuator displacement and magnitude of wing flapping. By using the Moticont voice coil motor (LVCM-010-013-01), with the actuator full stroke displacement from -1.8 mm to 1.5 mm (compression motion is negative and stretch motion is positive), as desired, the transmission generates analog linear motion to wing rotation. Moreover, the blue line is the transmission kinematics at statics from the experiment. Besides, the designed full stroke data is 6.4 mm; however, because of the re-design of the motor and assembly, our full stroke at statics is 3.3 mm as shown in Fig. 2.5b. To derive the experimental data for flapping wing magnitude sweeping with motor displacement, we glued (glue gun) the feet of flapping robot on the table and put a ruler into the frame of our high speed camera (Phantom-VEO-L) with 400 fps. After excited the actuator with pretty low velocity, we acquired the blue data line in Fig. 2.5b.

3.1.2 Elastic-energy exchange of the robot wingbeat

For effective elastic energy exchange, the system should be operated at the resonant frequency of the spring transmission and wing inertia [1]. For the voice coil motor case, We fixed the feet of one of our flapping robots on a scale (PMW-320, Intelligent Weighing Technology Laboratory Balance) and driving the voltage at

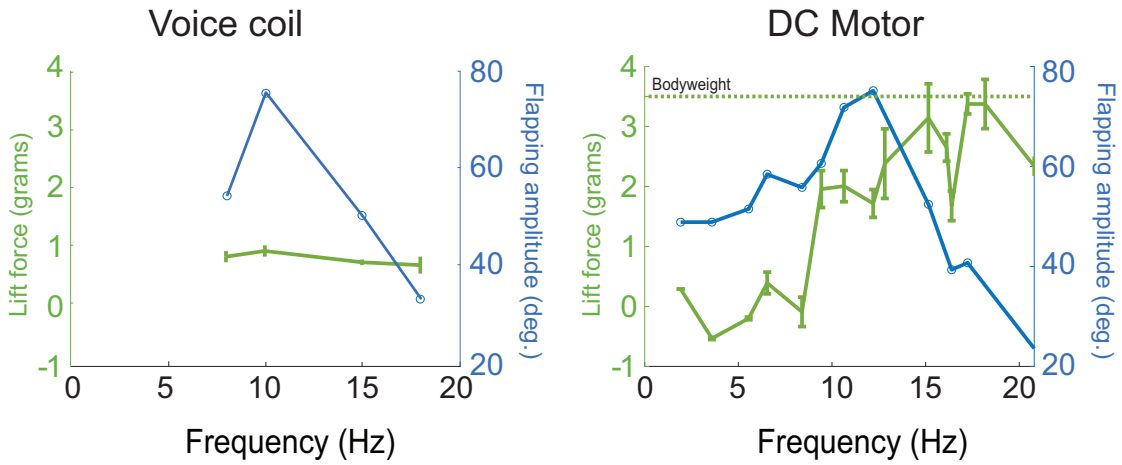

Figure 3.1: Lift force and flapping amplitude vs frequency for the voice coil driven robot and the rotary motor driven robot. Both show a resonant peak characteristic of elastic energy exchange, but the rotary motor produces significantly higher lift. The dashed green line indicates the weight support lift threshold

31V, we found out the the maximum magnitude of flapping wings is corresponding with maximum lift force, as shown in Fig. 3.1a, and the error bar is the standard deviation value in the data set at each frequency. Then, we go further and deeper to test the rotary motor case. After we fixed the robot body onto the force sensor (as shown in the Fig. 3.3a), and we found that the maximum lift force needs higher frequency than the need of the maximum flapping amplitude. Usually the lift force peak and the amplitude resonance don't coincide. This phenomena was introduced and studied by Zhang and Deng [33].

Furthermore, there are multiple "resonances" associated with different kinematic and dynamic variables. The kinematic resonance is where wingbeat amplitude is maximized as a function of frequency, ω. The lift resonance is where mean lift force is maximized as a function of frequency. These two resonance often don't

coincide, and instead the lift resonance is always at a higher frequency than the kinematics resonance. This occurs because if wingbeat amplitude is $G(\omega)$, than lift scales as $G(\omega)\omega^2$ and thus when the frequency is increased past the kinematic resonance (and thus $G(\omega)$ starts to decrease) the lift force will still increase a bit before decreasing.

Moreover, based on the rotary motor test, the frequency = 5/4 voltage. Thus, the higher maximum lift force can be generated at around 12V rather than 31V from voice coil case. And we can conclude that, the rotary motor performance better at lift force and flapping amplitude than voice coil motor case.

Besides, take Fig. 2.5a for example, the higher thickness of the compliant joints on the silicone transmission not only refers to higher blocked force, but also it has lower resonance frequency with higher damper performance. Thus, to have a better efficiency on elastic energy exchange, we followed the idea that keeping our thickness relatively low.

3.1.3 Free lift off

We next attempted to achieve take off from the ground and air. We placed the robot on the brass rails(shown in Fig. 3.3) and video recorded with a high-speed camera (Phantom-VEO-L) at 2000 frames per second. The actuator was driven at a voltage from 8V to 11v, that means the frequency excited roughly from 10Hz to 13.75Hz . In Fig. 3.2, we show an example take off from a robot on vertical rails to only allow vertical motion, and in the supplemental movie, we also show another

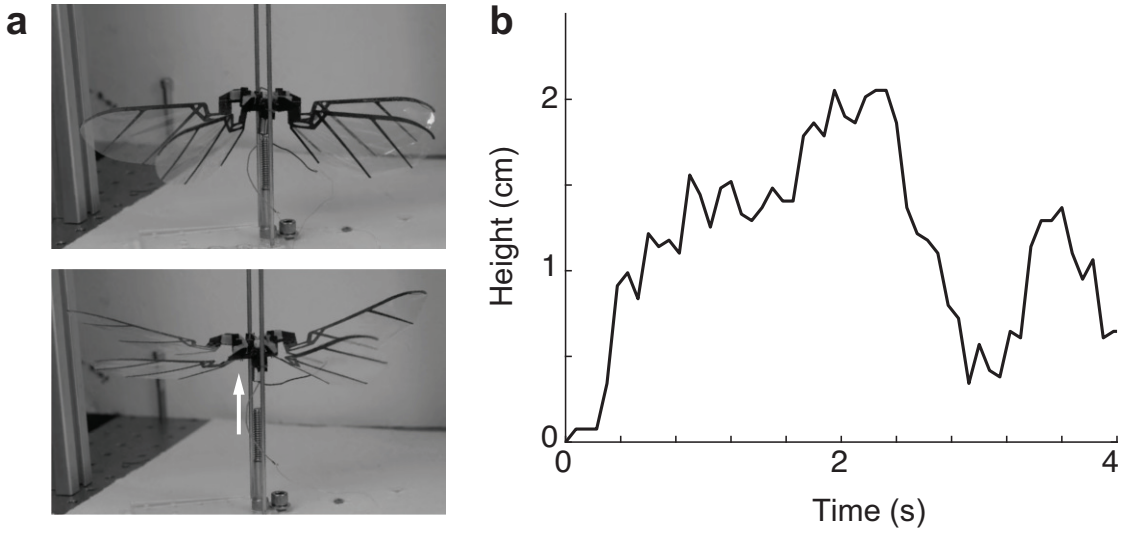

Figure 3.2: a) Two frames from Supplemental Movie, showing the robot's lift-off on a tethered rail. b) Height versus time during flapping.

take off experiment from a hanging robot (i.e. no leg bouncing effects). Since the robot is not under closed loop control flight is very unstable and in all takeoff attempts the robot would quickly roll or pitch. However, free take off experiments consistently demonstrated the robustness of the robot design. The compliance of the transmission was able to absorb the actuator motion and keep the wings from sustaining too much damage. This prompted us to explore how the transmission can act as an underactuated mechanisms to distribute load between wings that may get blocked by obstructions.

3.1.4 Robustness of the robot wingbeat

The rigid kinematics transmission always stopped moving when collision happened. Especially for four wings with rigid transmission, if they blocked one single

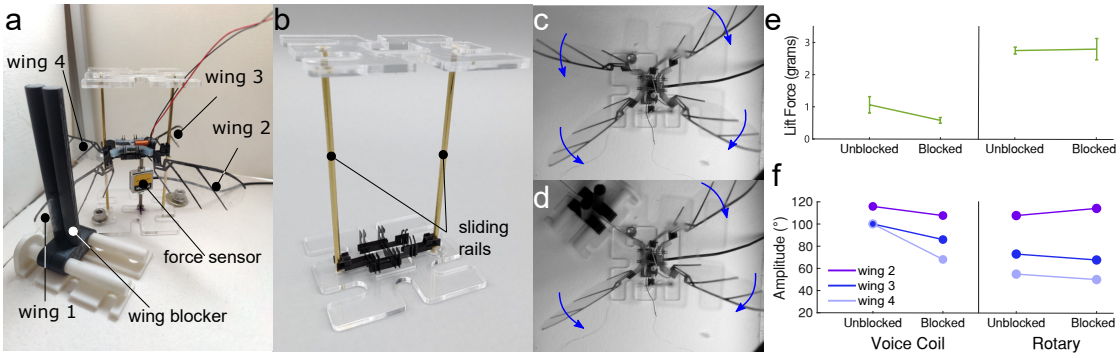

Figure 3.3: Overview of robustness test. (a) Detail of measurement setup with wings and wing blocker labeled (b) The brass sliding rails on either side of the chassis restrict motion to vertical, reducing anomalous force sensor measurements. The underactuated design of the transmission means that flapping is possible even when one wing is restricted (c & d). (e) Lift can be produced even when a wing is blocked, although the rotary motor performs better than the voice coil motor. (f) Both voice coil and rotary designs maintain significant wingbeat amplitudes, but fabrication inconsistencies make it difficult to achieve symmetrical wingstrokes

wing movement, and the rest of three will stop moving. However, when we testing our soft silicone transmission with internal skeleton, we found that the rest of three wings will still moving even after we locked one wing.

Then, we try to go deeper to inspect the lift force (by using the Futek load cell MODEL LSB200, which is used for lifted force tests, and we drive this one degree of freedom load cell by device USB-6003 with 1000 Sample Rate and 100 Number of Samples.) and flapping magnitude of wings when we locked one single wing. When we barely attached one dimensional force sensor onto the bottom of our flapping robot with signal amplifier, we found the force data was always been ruined with the inertia force from the magnet core motion (front and back motion). Thus, we set sliding rail on motor front and back side to eliminate the magnet inertia

force. Initially, we used carbon fiber rod with carbon fiber circle gripper. However, the contact friction between carbon and carbon is high, and the circle gripper on two sliding rail will generate a big overturning moment. Thus, we utilized a kind of brass sliding rail (Ultra-Machinable 360 Brass Rod, 3/32" diameter) to low the contact friction, and designed two flat plate grippers orthogonally arranged on each sliding rail. Even with tiny fabrication and assemble errors on motor chassis and sliding rail on acrylic(0.138" thickness) plate, this orthogonal flat plate grippers will tolerate them. Besides, we designed a wings locker as tips on slider, to clamp the wing frame from two sides, and ensure there is no force goes to the downside from the locker to the wing and finally to the force sensor.

As shown in the Fig. 3.3e is the mean lift force in one period with 12Hz frequency, which is the maximum flapping amplitude in Fig. 3.2b And in Fig. 3.3f, with the locked Wing 1, Wings 2-4 shows different performance in flapping magnitude.

Chapter 3, in full, is a reprint of the material as it appears in The IEEE Robotics and Automation Letters 2022. Hang Gao; James Lynch; Nick Gravish. The thesis author was the primary investigator and author of this paper.

Chapter 4

Discussion

4.1 Discussion

We have developed a novel flapping wing robot with a compliant transmission fabricated using a hybrid SCM and silicone molding technique, driven by a voice coil linear motor. We performed a range of benchtop experiments to characterize each of the components of the system. The full system has a characteristic resonant frequency that maximizes wingbeat amplitude and lift force, and it is able to achieve lift off for brief periods of time. The robot, like other FWMAVs, is unstable - it could not maintain open-loop flight - but it also has the unique feature of being able to continue to generate wing motion and lift even if one wing is restricted thanks to the compliant transmission.

One major challenge to achieving sustained flight in this robot is that we required high power input even to achieve brief lift off. We found that we could

generate significant lift, but only if we drove the motor at voltages that would cause it to burn out within a matter of seconds. This is primarily due to the inefficiencies in voice coil actuation [34]. Ultimately, further actuator development may be necessary to achieve successful implementation of this type of compliant transmission in an FWMAV.

The novel fabrication techniques we have used are part of a wider trend towards robustness and resilience in mobile robots. Robots like the 16g DASH robot [35] leverage lightweight materials and actuators to achieve high-speed running and resistance to damage from collisions and falls. Others use soft-robotic and compliant structures to build robots that are resistant to crushing and can navigate tight spaces [36–38]. Other researchers have incorporated bio-inspired collapsible wing features into flapping robots [39] that are able to dampen collisions with obstacles. Our work extends the principles inherent to robust robotic design and applies it to the transmission of flapping-wing robots, where it has the potential to provide an new level of resilience to future small-scale flying robots.

Chapter 4, in full, is a reprint of the material as it appears in The IEEE Robotics and Automation Letters 2022. Hang Gao; James Lynch; Nick Gravish. The thesis author was the primary investigator and author of this paper.

Chapter 5

Conclusion

5.1 Conclusion and future work

Flapping-wing robots have been a critical focus in aerial robotics over the last fifteen years and the pace of development has been rapid. New actuators, power autonomy, and control capabilities have been demonstrated in flapping wing robots. However, unlike their biological counterparts (flying insects for example) flapping wing robots can suffer from a lack of robustness as due to the materials used and the rapid motions of the wings. In this work we develop a novel compliant transmission for flapping wing aerial vehicles that provides elastic energy exchange and robustness to flapping wing robots. We demonstrate elastic energy exchange and resiliency to wing collisions in this robot in experiment. These advances present new design opportunities for flapping wing robots that may soon have to operate in crowded and obstacle-laden aerial environments.

Chapter 5, in full, is a reprint of the material as it appears in The IEEE Robotics and Automation Letters 2022. Hang Gao; James Lynch; Nick Gravish. The thesis author was the primary investigator and author of this paper.

Bibliography

[1] C. P. Ellington, "The novel aerodynamics of insect flight: applications to micro-air vehicles," *J. Exp. Biol.*, vol. 202, no. 23, pp. 3439–3448, 1999.

[2] J. P. Whitney and R. J. Wood, "Conceptual design of flapping-wing micro air vehicles," *Bioinspir. Biomim.*, vol. 7, no. 3, p. 036001, Apr. 2012.

[3] K. Y. Ma, P. Chirarattananon, S. B. Fuller, and R. J. Wood, "Controlled flight of a biologically inspired, Insect-Scale robot," *Science*, May 2013.

[4] Z. Tu, F. Fei, J. Zhang, and X. Deng, "Acting Is Seeing: Navigating Tight Space Using Flapping Wings," in *2019 International Conference on Robotics and Automation (ICRA)*, May 2019, pp. 95–101.

[5] N. T. Jafferis, E. F. Helbling, M. Karpelson, and R. J. Wood, "Untethered flight of an insect-sized flapping-wing microscale aerial vehicle," *Nature*, vol. 570, no. 7762, pp. 491–495, 2019.

[6] H. V. Phan, T. Kang, and H. C. Park, "Design and stable flight of a 21 g insect-like tailless flapping wing micro air vehicle with angular rates feedback control," *Bioinspir. Biomim.*, vol. 12, no. 3, p. 036006, Apr. 2017.

[7] Z. Tu, F. Fei, and X. Deng, "Untethered Flight of an At-Scale Dual-Motor Hummingbird Robot With Bio-Inspired Decoupled Wings," *IEEE Robotics and Automation Letters*, vol. 5, no. 3, pp. 4194–4201, Jul. 2020.

[8] S. B. Fuller, M. Karpelson, A. Censi, K. Y. Ma, and R. J. Wood, "Controlling free flight of a robotic fly using an onboard vision sensor inspired by insect ocelli," *J. R. Soc. Interface*, vol. 11, no. 97, p. 20140281, Aug. 2014.

[9] K. Jayaram, N. T. Jafferis, N. Doshi, B. Goldberg, and R. J. Wood, "Concomitant sensing and actuation for piezoelectric microrobots," *Smart Mater. Struct.*, vol. 27, no. 6, p. 065028, May 2018.

[10] C. De Wagter, S. Tijmons, B. D. W. Remes, and G. C. H. E. de Croon, "Autonomous flight of a 20-gram flapping wing MAV with a 4-gram onboard

stereo vision system," in *2014 IEEE International Conference on Robotics and Automation (ICRA)*. Hong Kong, China: IEEE, 2014, pp. 4982–4987.

[11] C. Laschi, B. Mazzolai, and M. Cianchetti, "Soft robotics: Technologies and systems pushing the boundaries of robot abilities," *Science robotics*, vol. 1, no. 1, p. eaah3690, 2016.

[12] S. O. Andersen and T. Weis-Fogh, "Resilin. a rubberlike protein in arthropod cuticle," in *Advances in Insect Physiology*, J. W. L. Beament, J. E. Treherne, and V. B. Wigglesworth, Eds. Academic Press, Jan. 1964, vol. 2, pp. 1–65.

[13] J. Michels, E. Appel, and S. N. Gorb, "Functional diversity of resilin in arthropoda," *Beilstein J. Nanotechnol.*, vol. 7, pp. 1241–1259, Sep. 2016.

[14] J. Gau, N. Gravish, and S. Sponberg, "Indirect actuation reduces flight power requirements in manduca sexta via elastic energy exchange," *J. R. Soc. Interface*, vol. 16, no. 161, p. 20190543, Dec. 2019.

[15] A. M. Mountcastle and S. A. Combes, "Biomechanical strategies for mitigating collision damage in insect wings: structural design versus embedded elastic materials," *J. Exp. Biol.*, vol. 217, no. 7, 2014.

[16] T. Deora, N. Gundiah, and S. P. Sane, "Mechanics of the thorax in flies," *J. Exp. Biol.*, vol. 220, no. Pt 8, pp. 1382–1395, Apr. 2017.

[17] S. S. Baek, K. Y. Ma, and R. S. Fearing, "Efficient resonant drive of flapping-wing robots," in *2009 IEEE/RSJ International Conference on Intelligent Robots and Systems*. St. Louis, MO, USA: IEEE, 2009, pp. 2854–2860.

[18] D. Campolo, M. Azhar, G.-K. Lau, and M. Sitti, "Can DC motors directly drive flapping wings at high frequency and large wing strokes?" *IEEE/ASME Trans. Mechatron.*, vol. 19, no. 1, pp. 109–120, Feb. 2014.

[19] Y. Zou, W. Zhang, and Z. Zhang, "Liftoff of an electromagnetically driven insect-inspired flapping-wing robot," *IEEE Trans. Rob.*, vol. 32, no. 5, pp. 1285–1289, 2016.

[20] Y. Chen, H. Zhao, J. Mao, P. Chirarattananon, E. F. Helbling, N.-S. P. Hyun, D. R. Clarke, and R. J. Wood, "Controlled flight of a microrobot powered by soft artificial muscles," *Nature*, vol. 575, no. 7782, pp. 324–329, Nov. 2019.

[21] R. Sahai, K. C. Galloway, and R. J. Wood, "Elastic element integration for improved Flapping-Wing micro air vehicle performance," *IEEE Trans. Rob.*, vol. 29, no. 1, pp. 32–41, Feb. 2013.

[22] T. Weis-Fogh, "Quick estimates of flight fitness in hovering animals, including novel mechanisms for lift production," *J. Exp. Biol.*, vol. 59, no. 1, pp. 169–230, Aug. 1973.

[23] C. Chen and T. Zhang, "A review of design and fabrication of the bionic flapping wing micro air vehicles," *Micromachines*, vol. 10, no. 2, p. 144, 2019.

[24] N. O. Pérez-Arancibia, K. Y. Ma, K. C. Galloway, J. D. Greenberg, and R. J. Wood, "First controlled vertical flight of a biologically inspired microrobot," *Bioinspir. Biomim.*, vol. 6, no. 3, p. 036009, Sep. 2011.

[25] M. H. Rosen, G. le Pivain, R. Sahai, N. T. Jafferis, and R. J. Wood, "Development of a 3.2g untethered flapping-wing platform for flight energetics and control experiments," in *2016 IEEE International Conference on Robotics and Automation (ICRA)*. Stockholm, Sweden: IEEE, 2016, pp. 3227–3233.

[26] R. J. Wood, S. Avadhanula, R. Sahai, E. Steltz, and R. S. Fearing, "Microrobot design using fiber reinforced composites," 2008.

[27] J. G. Cham, S. A. Bailey, J. E. Clark, R. J. Full, and M. R. Cutkosky, "Fast and robust: Hexapedal robots via shape deposition manufacturing," *Int. J. Rob. Res.*, vol. 21, no. 10-11, pp. 869–882, Oct. 2002.

[28] W. Zhou and N. Gravish, "Soft microrobotic transmissions enable rapid Ground-Based locomotion," in *2020 IEEE/RSJ International Conference on Intelligent Robots and Systems (IROS)*. Las Vegas, NV, USA: IEEE, Oct. 2020, pp. 7874–7880.

[29] M. K. Salcedo, J. Hoffmann, S. Donoughe, and L. Mahadevan, "Computational analysis of size, shape and structure of insect wings," *Biol. Open*, vol. 8, no. 10, Oct. 2019.

[30] Y. M. Chukewad, J. James, A. Singh, and others, "RoboFly: An insect-sized robot with simplified fabrication that is capable of flight, ground, and water surface locomotion," *IEEE Transactions on*, 2021.

[31] S. P. Sane, "The aerodynamics of insect flight," *J. Exp. Biol.*, vol. 206, no. 23, pp. 4191–4208, Dec. 2003.

[32] J. A. Roll, B. Cheng, and X. Deng, "An Electromagnetic Actuator for High-Frequency Flapping-Wing Microair Vehicles," *IEEE Trans. Rob.*, vol. 31, no. 2, pp. 400–414, Apr. 2015.

[33] J. Zhang and X. Deng, "Resonance principle for the design of flapping wing micro air vehicles," *IEEE Trans. Rob.*, vol. 33, no. 1, pp. 183–197, Feb. 2017.

[34] E. Farrell Helbling and R. J. Wood, "A review of propulsion, power, and control architectures for Insect-Scale Flapping-Wing vehicles," *Appl. Mech. Rev.*, vol. 70, no. 1, p. 010801, 2018.

[35] P. Birkmeyer, K. Peterson, and R. S. Fearing, "DASH: A dynamic 16g hexapedal robot," in *2009 IEEE/RSJ International Conference on Intelligent Robots and Systems*, Oct. 2009, pp. 2683–2689.

[36] M. T. Tolley, R. F. Shepherd, B. Mosadegh, K. C. Galloway, M. Wehner, M. Karpelson, R. J. Wood, and G. M. Whitesides, "A resilient, untethered soft robot," *Soft Robotics*, vol. 1, no. 3, pp. 213–223, Sep. 2014.

[37] K. Jayaram and R. J. Full, "Cockroaches traverse crevices, crawl rapidly in confined spaces, and inspire a soft, legged robot," *Proc. Natl. Acad. Sci. U. S. A.*, vol. 113, no. 8, pp. E950–7, Feb. 2016.

[38] Y. Wu, J. K. Yim, J. Liang, Z. Shao, M. Qi, J. Zhong, Z. Luo, X. Yan, M. Zhang, X. Wang, R. S. Fearing, R. J. Full, and L. Lin, "Insect-scale fast moving and ultrarobust soft robot," *Sci Robot*, vol. 4, no. 32, Jul. 2019.

[39] A. M. Mountcastle, E. F. Helbling, and R. J. Wood, "An insect-inspired collapsible wing hinge dampens collision-induced body rotation rates in a microrobot," *J. R. Soc. Interface*, vol. 16, no. 150, p. 20180618, Jan. 2019.